Circular-Arc Line Arrays with Amplitude Shading for Constant Directivity*

RICHARD TAYLOR†, *AES Member*
rtaylor@tru.ca

Thompson Rivers University, Kamloops, Canada

KURTIS MANKE,
kurtismanke123@gmail.com

University of Victoria, Victoria, Canada

AND D. B. (DON) KEELE, JR., *AES Fellow*
DKeeleJr@comcast.net

DBK Associates and Labs, Bloomington, IN 47408, USA

We develop the theory for a constant-beamwidth transducer (CBT) formed by an unbaffled, continuous circular-arc isophase line source. Appropriate amplitude shading of the source distribution leads to a far-field radiation pattern that is constant above a cutoff frequency determined by the prescribed beam width and arc radius. We derive two shading functions, with cosine and Chebyshev polynomial forms, optimized to minimize this cutoff frequency and thereby extend constant-beamwidth behavior over the widest possible band. We illustrate the theory with simulations of magnitude responses, full-sphere radiation patterns and directivity index, for example arrays with both wide- and narrow-beam radiation patterns. We further extend the theory to describe the behavior of circular-arc arrays of discrete point sources.

0 Introduction

There is much interest in the design of acoustic sources whose radiation pattern is substantially independent of frequency. Such a source exhibits constant directivity [2]—a weaker criterion that is often used in practice. Much of this interest stems from work by Toole and others (see [3] and references therein) showing that constant directivity is correlated with subjective perception of quality in stereo reproduction. Constant directivity beamforming also has wide application to sensor and transducer arrays in audio, broadband sonar, ultrasound imaging, and radar and other remote sensing applications [4, 5, 6, 7].

Keele [8, 9, 10, 11, 12] has reported extensively on a constant-beamwidth transducer (CBT) formed by a circular-arc array with amplitude shading. That work followed on that of Rogers and Van Buren [4] who showed that a transducer with frequency-independent beam pattern can be formed by a spherical cap with amplitude shading based on a Legendre function. Fortuitously, when Legendre shading is used on a circular arc, a substantially frequency-independent radiation pattern results in that case as well [8, 9].

Despite the demonstrated advantages of circular-arc CBT line arrays, to date there has not been a theoretical account of Keele's empirical results. Legendre shading in particular has been given only *post hoc* justification; shading functions adapted to circular arrays have not been developed.

Circular arrays have been analyzed extensively in the EM antenna literature [13, 14, 15] but there they seem to have been regarded as narrow-band transducers only [14, p. 192]. Several authors have considered circular arc arrays with *uniform* excitation [16, 17, 18] but these do not perform well as broadband radiators. In the audio field there has been significant work on beam-forming techniques for

*An early version of this paper was presented at the 143rd Convention of the Audio Engineering Society, New York NY, 18-20 Oct. 2017, under the title "Theory of Constant Directivity Circular-Arc Line Arrays" [1]; revised June 2018.

†Correspondence should be addressed to R. Taylor; tel: +1-250-371-5987; e-mail: rtaylor@tru.ca

circular arrays of both microphones [6, 7, 19, 20, 21, 22] and loudspeakers [23, 24, 25, 26, 27, 28, 29]. However, the potential for broadband constant directivity via a simple frequency-independent amplitude-only shading of an unbaffled circular-arc array does not appear to be widely known.

The aims of the present work are twofold: to provide a theoretical foundation to account for the observed constant-directivity behavior of amplitude-shaded circular-arc arrays, and to derive improved shading functions adapted to these arrays. The paper is structured as follows. In the following section we review the theory for acoustic radiation from an amplitude-shaded, unbaffled circular arc. We then use this theory to derive conditions on the shading function that guarantee a frequency-independent radiation pattern. On this basis, in Sec. 2 we develop suitable families of optimal shading functions that can be used to synthesize a wide variety of radiation patterns. In Sec. 3 we present results of simulations that illustrate and confirm several key aspects of our theory. Sec. 4 shows how our theory can be extended to treat discrete arrays.

1 Theory

1.1 Radiation from a Circular Array

Consider a time-harmonic line source in the form of a circle of radius a in free space, as shown in Fig. 1. The circle lies in the horizontal xy-plane with its center at the origin. (This orientation facilitates use of conventional spherical coordinates; in Keele's prior work [8, 9] the array is oriented vertically.) We take the x-axis ($\theta = \phi = 0$) as the "on-axis" direction of the resulting radiation pattern. We assume the source distribution is continuous and iso-phase, with amplitude that varies with polar angle α according to a dimensionless, real-valued and frequency-independent *shading function* $S(\alpha)$ (often called the *amplitude taper* or *aperture function* in the EM antenna literature). It proves convenient to consider a full circular array at first; later we restrict the active part of the array to an arc by setting $S(\alpha)$ to zero on part of the circle.

Referring to Fig. 1, consider a representative point source element at Q with time-dependence $e^{i\omega t}$. The radiated pressure at O is then e^{-ikR}/R (up to a multiplicative constant) where k is the wave number [30, p. 311]. Summing the pressure contributions at O from all elements of the array gives the total pressure p via the Rayleigh-like integral

$$p(r,\theta,\phi) = \int_0^{2\pi} S(\alpha)\frac{e^{-ikR}}{R}\,d\alpha \tag{1}$$

where

$$\begin{aligned} R &= \sqrt{a^2 + r^2 - 2ar\cos\phi\cos(\theta-\alpha)} \\ &\approx r - a\cos\phi\cos(\theta-\alpha) \qquad (r \gg a). \end{aligned} \tag{2}$$

On making the usual far-field ($r \gg a$) approximations eq. (1) gives

$$p = \frac{e^{-ikr}}{r}\int_0^{2\pi} S(\alpha)e^{ika\cos\phi\cos(\theta-\alpha)}\,d\alpha \tag{3}$$

We will assume that the shading function $S(\alpha)$ has even symmetry about $\alpha = 0$ so it can be expressed as a Fourier cosine series

$$S(\alpha) = \sum_{n=0}^{\infty} a_n \cos n\alpha \tag{4}$$

(the EM antenna literature calls this an expansion in *amplitude modes* or *circular harmonics*, as opposed to the phase modes $e^{in\alpha}$ [31].) In the following we refer to each term in eq. (4) as a *shading mode*. Substituting eq. (4) into (3) gives the far-field pressure radiated by a circular array (with $u = \theta - \alpha$),

$$\begin{aligned} p &= \frac{e^{-ikr}}{r}\int_0^{2\pi}\sum_{n=0}^{\infty} a_n \cos\big(n[u+\theta]\big)e^{ika\cos\phi\cos u}\,du \\ &= \frac{e^{-ikr}}{r}\sum_{n=0}^{\infty} a_n\Bigg[\cos(n\theta)\underbrace{\int_0^{2\pi}\cos(nu)e^{ika\cos\phi\cos u}\,du}_{2\pi i^n J_n(ka\cos\phi)} \\ &\qquad - \sin(n\theta)\underbrace{\int_0^{2\pi}\sin(nu)e^{ika\cos\phi\cos u}\,du}_{0}\Bigg] \\ &= \frac{e^{-ikr}}{r}\sum_{n=0}^{\infty} a_n f_n(ka\cos\phi)\cos n\theta, \end{aligned} \tag{5}$$

where the *radiation mode amplitudes* f_n are given by

$$f_n(x) = 2\pi i^n J_n(x) \tag{6}$$

and J_n is a Bessel function of the first kind [32], with $x \equiv ka\cos\phi$. Note that the frequency enters only via the dimensionless quantity ka which is the ratio of array circumference to wavelength, i.e. the "acoustic size" of the array. Fig. 2 plots the first several mode amplitudes $|f_n(ka)|$ (in the plane of the array $\phi = 0$) as a function of frequency.

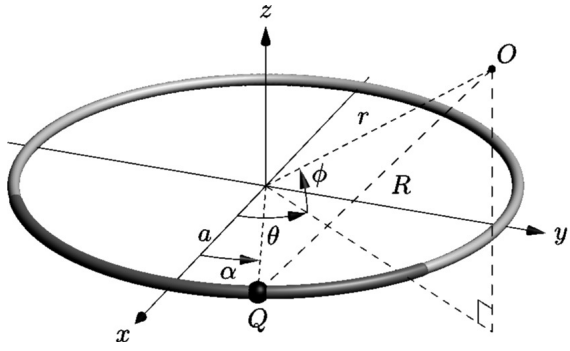

Fig. 1: Circular line source geometry. The shaded arc is the active part of the array considered in the balance of the paper.

Eq. (6) for the mode amplitudes of an unbaffled circular array appears throughout the literature on circular arrays of sources and receivers [7, 13, 15, 31, 33]. We have included its derivation here in the interest of a self-contained presentation, and to avoid confusion that might result from different coordinate systems used in other works. It should be noted that this expression for the mode amplitudes is

essentially unchanged if, instead of the cosine series of eq. (4), the shading function is expressed as a sum of complex Fourier modes $a_n e^{in\alpha}$, as is often the case elsewhere in the literature.

If the array is mounted on an axisymmetric baffle then only the formula for the mode amplitudes changes. Closed-form expressions for the mode amplitudes when the baffle is in the form of a sphere, or a finite- or infinite-length cylinder, are collected in [7]. The case of a circular-arc array in the corner of a wedge-shaped propagation space is treated analytically in [29].

Eq. (5) reveals much about the behavior of circular arrays:

- Each $\cos n\alpha$ shading mode gives rise to a corresponding far-field radiation mode of the same $\cos n\theta$ polar form. Eq. (5) represents the total far-field pressure as a superposition of these radiation modes.
- Each shading mode is mapped to the far field by a factor $f_n(ka\cos\phi)$ that determines its radiation strength. It is apparent in Fig. 2 that each shading mode exhibits a series of nulls (comb filtering) in its magnitude response. Physically, these nulls are caused by destructive interference between source elements on opposite sides of the array. Eqs. (5)–(6) show that the nulls occur where $ka\cos\phi$ coincides with a zero of the Bessel function J_n.
- Owing to these nulls, a full-circle array with amplitude shading $S(\alpha) = \cos n\alpha$ cannot produce a usable broadband response: at any point in the far field there are frequencies at which the radiated pressure is zero. This is the "mode stability" problem inherent to circular arrays [15]. Nevertheless, in Sec. 1.3 we show that limiting the active part of the array to an arc of less than 180° gives a well-behaved broadband response.

1.2 Limiting Cases

1.2.1 Low Frequency

At low frequency we can use the asymptotic form [32]

$$J_n(x) \approx \frac{1}{n!}\left(\frac{x}{2}\right)^n \qquad (x \ll 1) \tag{7}$$

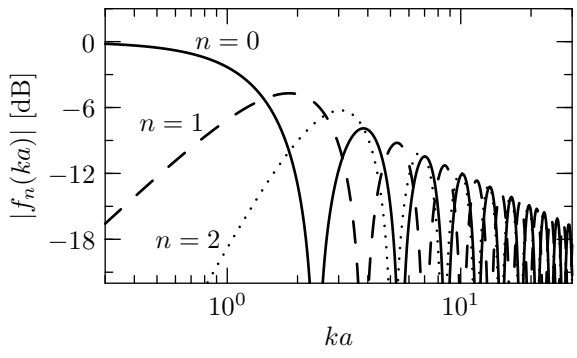

Fig. 2: Mode amplitudes: on-axis far-field pressure, as a function of dimensionless frequency ka, for radiation from a circular array with $\cos(n\alpha)$ amplitude shading.

in eq. (5) to obtain the far-field pressure

$$p \approx 2\pi \frac{e^{-ikr}}{r} \sum_{n=0}^{\infty} a_n \frac{i^n (ka)^n}{2^n n!} \cos^n\phi \cos(n\theta) \quad (ka \ll 1). \tag{8}$$

Thus the strength of the nth radiation mode falls off as $(ka)^n$ (hence $6n$ dB/oct) toward low frequency, as illustrated in Fig. 2. All modes with $n > 0$ radiate inefficiently at low frequency. At low frequency ($ka \to 0$) the limiting radiation pattern is determined by the leading-order term in (8). In particular, if $a_0 \neq 0$ then the low-frequency pattern is omni-directional: the array radiates like a point source at the origin. Alternatively, if $a_0 = 0$ but $a_1 \neq 0$ then the array exhibits dipole radiation at low frequency.

1.2.2 High Frequency

Using the asymptotic form [32]

$$J_n(x) \approx \sqrt{\frac{2}{\pi x}} \cos(x - n\tfrac{\pi}{2} - \tfrac{\pi}{4}) \quad (x \gg n) \tag{9}$$

in eq. (6) gives a high-frequency approximation for the mode amplitudes,

$$f_n(x) \approx \sqrt{\frac{8\pi}{x}} \begin{cases} \cos(x - \frac{\pi}{4}) & n \text{ even} \\ i\sin(x - \frac{\pi}{4}) & n \text{ odd.} \end{cases} \tag{10}$$

Note that the nulls of even-order modes coincide with peaks of the odd-order modes, and vice versa; this observation plays a key role in the following section.

1.3 Conditions for Constant Radiation Pattern

At sufficiently high frequency, such that $x \equiv ka\cos\phi \gg n$ for all non-negligible terms in the Fourier expansion of the shading function in eq. (4), we can substitute the limiting form from eq. (10) into (5) to obtain the far-field pressure

$$p \approx \frac{e^{-ikr}}{r}\sqrt{\frac{8\pi}{x}}\left[S_e(\theta)\cos(x - \tfrac{\pi}{4}) + iS_o(\theta)\sin(x - \tfrac{\pi}{4})\right] \tag{11}$$

where

$$S_e(\theta) = \sum_{n\ \text{even}} a_n \cos n\theta, \quad S_o(\theta) = \sum_{n\ \text{odd}} a_n \cos n\theta. \tag{12}$$

Eq. (11) gives the pressure magnitude

$$|p| = \frac{1}{r}\sqrt{\frac{8\pi}{x}}\sqrt{S_e^2(\theta)\cos^2(x - \tfrac{\pi}{4}) + S_o^2(\theta)\sin^2(x - \tfrac{\pi}{4})}. \tag{13}$$

Eq. (13) has a simple physical interpretation: with increasing frequency the polar pattern in the plane of the array alternates periodically between the odd- and even-order patterns $|S_o(\theta)|$ and $|S_e(\theta)|$. In particular, if $|S_e(\theta)| = |S_o(\theta)|$ for all θ then the radiation pattern is unchanging with frequency; in this case eq. (13) gives the far-field pressure

$$|p(r,\theta,\phi)| = \frac{1}{r}\sqrt{\frac{8\pi}{ka}}\frac{|S_e(\theta)|}{\sqrt{\cos\phi}}. \tag{14}$$

Critically for our purposes **the amplitude of this radiation pattern varies with frequency but its polar pattern does not**.

Thus, the far-field radiation pattern of a circular array will be independent of frequency provided the amplitude shading function $S(\alpha)$ satisfies the following conditions:

1. $S = S_o + S_e$ with S_o, S_e given by eq. (12) and satisfying $|S_o| = |S_e|$.
2. For all non-negligible coefficients a_n in the cosine series for S we have $ka\cos\phi \gg n$.

(These conditions are identical to those given in [5] for radiation from a spherical array, except in that case the a_n are coefficients of the shading function expanded in spherical harmonics.)

In Appendix A.1 we show that condition 1 is equivalent to requiring that, for each θ, at most one of $S(\theta)$ and $S(\pi-\theta)$ is non-zero. This holds e.g. if the active part of the array is restricted to an arc of 180° or less. This in turn implies the radiation pattern

$$|p(r,\theta,\phi)| = \frac{1}{r}\sqrt{\frac{2\pi}{ka\cos\phi}}\begin{cases}|S(\theta)| & -\frac{\pi}{2} < \theta < \frac{\pi}{2} \\ |S(\pi-\theta)| & \frac{\pi}{2} < \theta < \frac{3\pi}{2}.\end{cases} \tag{15}$$

Several remarks are in order:

- Conditions 1 and 2 together ensure a constant radiation pattern above a certain *cutoff frequency* determined by the requirement that $ka\cos\phi \gg n_{\max}$ where $n_{\max}$ is the largest n for which the shading mode amplitude a_n is non-negligible. For greater out-of-plane angles ϕ the cutoff frequency is correspondingly higher.
- Above cutoff, eq. (14) predicts a well-behaved response without the nulls present in the individual radiation modes. Indeed, the condition $|S_e(\theta)| = |S_o(\theta)|$ ensures that the response nulls of the odd-order modes are exactly filled in by peaks of the even-order modes, and vice versa (see remark in Sec. 1.2.2).
- The limiting radiation pattern given by eq. (14) is bi-directional and symmetric across the *yz*-plane in Fig. 1 (see Appendix A.1).
- The radiation pattern in eq. (14) is unchanged if the shading is reflected across the *yz*-plane. Thus, in the far field it is immaterial whether it is the "front" or "back" side of the array that is active.
- Provided the active part of the array is restricted to an arc of 180° or less, eq. (15) shows that the limiting radiation pattern is *identical to the shading function* in any plane parallel to the array (constant ϕ).
- Eq. (14) predicts a smooth $(ka)^{-1/2}$ (hence -3 dB/oct) magnitude response everywhere in the far field. As noted in [10], in a practical device this high-frequency rolloff may require compensatory equalization. The required 3 dB/oct equalizer response (i.e. a blueing filter) can be well-approximated by a low-Q high-pass shelving filter, or by swapping poles with zeroes of any of the well-known pinking fiters [34].
- Eq. (15) shows that the limiting high-frequency pattern is the product of an in-plane pattern (identical to the shading function) and a broad $1/\sqrt{\cos\phi}$ out-of-plane pattern. The out-of-plane pattern exhibits amplitude peaks on the z-axis perpendicular to the circular array. These peaks are due to the fact that radiation from all elements of the array arrives in-phase on the z-axis; elsewhere there is some destructive interference among source elements. This interference increases with frequency, causing the 3 dB/oct rolloff noted above.
- To minimize the cutoff frequency (and thereby achieve a constant radiation pattern over the widest possible band) we need a shading function whose Fourier coefficients a_n are of the lowest order possible. Sec. 2 considers the design of such a function.

Each of these theoretical results has been corroborated by Keele's extensive simulations and measurements of circular-arc CBT arrays [8, 9, 10, 12].

1.4 Discussion

Careful consideration of Fig. 2 together with eq. (5) (and the limiting cases given by eqs. (8) and (14)) yields a complete characterization of the radiating behavior of an amplitude-shaded circular-arc array.

In the low-frequency limit ($ka \ll 1$) only the $n = 0$ shading mode radiates into the far field. Directivity control is lost below the array's cutoff frequency: the array behaves as a point source, with omni-directional radiation pattern. (By contrast, beam-forming can achieve significant directivity even at low frequency [23, 24, 25, 26, 27], but with much higher implementation complexity and requiring a large amount of compensatory gain.)

With increasing frequency, successively higher-order shading modes begin to "turn on" and contribute to the far-field radiation pattern. The superposition of radiation modes in eq. (5) yields a radiation pattern that changes with frequency throughout a transition band around $ka \approx 1$ (i.e. as the array goes from being acoustically small to large).

Above the array's cutoff frequency ($ka \approx n_{\max}$) all shading modes are actively radiating into the far field. The superposition of radiation modes generates the frequency-independent, bi-directional pattern given by eq. (14). With increasing frequency above cutoff there are no further shading modes to "turn on", so that the radiation pattern ceases to change; this is the physical origin of constant directivity behavior of circular-arc (CBT) arrays.

In other words, a circular array acts as a low-pass spatial filter that determines which shading modes pass to the far-field response (see e.g. [15, p. 27]). The bandwidth of this filter varies with acoustic frequency: at any given frequency, shading modes of order $n < ka$ pass through to the far field; higher-order modes $n > ka$ are strongly attenuated (cf. Fig. 2). As the frequency increases the filter's pass-band widens, passing modes of sequentially higher order. If a finite number of Fourier modes are present in the shading function, then at sufficiently high frequency all these modes will fall within the filter's pass-band; the

shading function is then replicated in the far field and the radiation pattern ceases to change with frequency.

For an array that is active only on an arc $|\theta| \le \theta_0$ we have $n_{\max} \approx \pi/(2\theta_0)$ (see App. A.2). In terms of the wavelength λ and array length $L = a2\theta_0$, the cutoff criterion $ka > n_{\max}$ can then be expressed as $\lambda < 2L$. Thus, as for linear and other array geometries, circular-arc arrays are able to achieve significant directivity only when the array is larger than the wavelength.

It should be noted that if the array is mounted on a long cylindrical baffle then the results above are essentially unchanged, but obtained more readily as a special case of the analysis carried out in [28]. Indeed, provided the mode amplitudes $f_n(ka) \equiv f(ka)$ become asymptotically independent of n for $ka \gg n_{\max}$ (as is the case for an infinitely long cylindrical baffle [26, 28]) eq. (5) for the radiation pattern gives

$$p = \frac{e^{-ikr}}{r} f(ka\cos\phi)S(\theta) \quad (ka \gg n_{\max}). \tag{16}$$

Thus the radiation pattern in the plane of the array is again frequency-independent and identical to the shading function. However, unlike the unbaffled case analyzed here (compare eqs. (15) and (16)) the shading function is not reflected into the rear radiation pattern, hence a baffled array enjoys greater directivity control. Also, in the baffled case the active part of the array need not be restricted to an arc of 180° or less.

2 Optimal Amplitude Shading

Keele [8] demonstrated that the choice of shading function is critical to achieving broadband constant directivity with a circular-arc array. As shown in the previous section, a good shading function $S(\theta)$ will have its Fourier spectrum concentrated in its lowest-order terms, while being non-zero only on an arc $|\theta| \le \theta_0 \le \frac{\pi}{2}$ (θ_0 determines the angular coverage of the active part of the array). The general form of such a shading function is shown in Fig. 3.

Legendre shading, developed for spherical arrays in [4], has been used to good effect by Keele in his work on CBT arrays [8, 9, 10, 11]. Since Legendre functions serve to minimize the amplitude of higher-order terms when the shading function is expanded in spherical harmonics [4] (which are themselves polynomials in $\cos\theta$) it is not surprising that Legendre function shading does a reasonably good job of satisfying the criteria outlined above. However, being adapted to a spherical rather than circular radiator, Legendre function shading is not the optimal choice. In the Appendices we develop two new shading functions with the goal of constant directivity over the widest possible band.

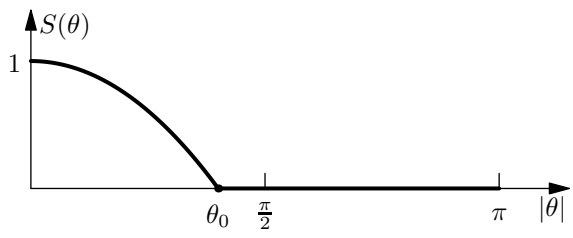

Fig. 3: Shading function restricted to the arc $|\theta| \le \theta_0$.

Appendix A.2 shows that the *cosine shading*

$$S(\theta) = \begin{cases} \cos\left(\frac{\pi}{2} \cdot \frac{\theta}{\theta_0}\right) & |\theta| \le \theta_0 \\ 0 & \theta_0 < |\theta| \le \pi \end{cases} \tag{17}$$

is optimal in that each of its Fourier coefficients $|a_n|$ is at a local minimum (as a function of θ_0) for all $n > \pi/(2\theta_0)$. This serves to concentrate the shading modes in the lowest orders.

Remarks

- The cosine shading (17) is analogous to (but much simpler than) the Legendre function $P_\nu(\cos\theta)$ developed in [4] and used elsewhere by Keele; they are identical in the case $\theta_0 = \frac{\pi}{2}$.
- The parameter θ_0 controls the beam width of the array. The design equations for cosine shading are particularly simple: we have $\theta_0 = \frac{3}{2}\theta_6$ where θ_6 is the desired off-axis angle at which the level falls to -6 dB. By contrast, the design equations for Legendre shading cannot be expressed in closed form, and require numerical root-finding as well as evaluation of the rather obscure Legendre functions.
- Decreasing θ_0 (narrowing the beam width) increases the index $n_{\max}$ above which the cosine series coefficients a_n are minimized; this leads to a higher cutoff frequency for a given arc radius.

Appendix A.3 shows that the *Chebyshev polynomial shading*

$$S(\theta) = \begin{cases} T_N\left(2 \cdot \frac{1+\cos\theta}{1+\cos\theta_0} - 1\right) & |\theta| \le \theta_0 \\ 0 & \theta_0 < |\theta| \le \pi, \end{cases} \tag{18}$$

where T_N is the Nth Chebyshev polynomial, is optimal in the sense that it is close to a degree-N polynomial in $\cos\theta$, so its Fourier coefficients a_n are concentrated in low orders $n \le N$. Chebyshev shading is in some ways superior to both cosine shading and the Legendre shading used in [8], as we illustrate in the following section. Together, the parameters N and θ_0 control the beam width and arc coverage. For a given coverage angle θ_0, increasing N results in a narrower beam.

A thorough comparison of these shading functions and their radiating behaviors is beyond the scope of this paper. We merely note in passing that cosine shading appears to allow for the widest possible beam pattern. Chebyshev shading can yield very narrow patterns and (especially for greater values of the polynomial order N) can achieve smoother frequency response at the expense of greater arc coverage. The following section presents detailed simulations of two representative examples.

3 Examples

To confirm and illustrate key aspects of our theoretical results above, here we present simulations of two particular circular-arc arrays designed to achieve broadband constant directivity, but with different beam widths. One is a wide-beam array with the cosine shading (see Appendix A.2)

$$S(\theta) = \begin{cases} \cos\left(\frac{9}{7}\theta\right) & |\theta| \le 70^\circ \\ 0 & |\theta| > 70^\circ \end{cases} \tag{19}$$

which falls to -6 dB at 47° off-axis. The other is a narrow-beam array with the degree-6 Chebyshev polynomial shading (see Appendix A.3)

$$S(\theta) = \begin{cases} T_6\left(2 \cdot \frac{1+\cos\theta}{1+\cos 52^\circ} - 1\right) & |\theta| \le 52^\circ \\ 0 & |\theta| > 52^\circ \end{cases} \tag{20}$$

which falls to -6 dB at 25°. Here the arc cutoff angles of 70° and 52° are rather arbitrary; they were chosen by trial and error to make the magnitude responses in Fig. 6 reasonably smooth.

The shading functions in eqs. (19)–(20) are plotted in Fig. 4, together with some other shading functions that achieve the same beam widths. Chebyshev shading, especially with higher polynomial degree, gives a more gradual taper near the end of the arc. This results in smoother frequency response (see Fig. 7 below) at the expense of requiring greater arc coverage for a given beam width.

3.1 Magnitude Response

Fig. 5 shows the raw (unequalized) far-field magnitude responses at various angles θ in the plane of an array with the narrow-beam shading of eq. (20). These were calculated by numerical quadrature (via an adaptive Simpson's rule) of the Rayleigh integral in eq. (3). (We ignore overall e^{-ikr}/r radial term in eq. (3), as our concern here is with the polar response.) The responses are plotted against the dimensionless frequency ka. (For reference, an array of radius $a = 1$ m has $ka = 1$ at 54 Hz.)

Fig. 5 illustrates several aspects of the theory developed above. There is a clear cutoff frequency ($ka \approx 10$) above which the radiation pattern transitions from omni-directional to a frequency-independent narrow beam pattern. Above cutoff the level rolls off at 3 dB/oct at all off-axis angles, as predicted by eq. (14). In marked contrast with a full-circle array (Fig. 2), this shaded circular arc provides a usable raw response at all frequencies, without nulls or significant ripples.

For both the wide-beam cosine shading (19) and narrow-beam Chebyshev shading (20), Fig. 6 shows the far-field magnitude responses at various angles θ in the plane of the array, this time normalized to the on-axis ($\theta = 0$) response. In agreement with our theory, above the cutoff frequency ($ka \approx 3$ for the wide-beam example; $ka \approx 10$ for the narrow-beam case) the normalized response becomes flat at all angles, indicating a constant radiation pattern.

To illustrate the improvement in Chebyshev over Legendre function shading, Fig. 7 shows the far-field magnitude response at various angles in the plane of the array, for two arrays shaded to achieve a -6 dB beam angle of 25°: one with Legendre function shading given in [8], the other with the degree-6 Chebyshev shading of eq. (20). The Legendre-shaded array exhibits response ripples of several dB, whereas the Chebyshev-shaded array has a ripple-free response at all off-axis angles. Moreover, with increasing frequency the Chebyshev-shaded array settles more quickly into a frequency-independent radiation pattern, particularly at angles beyond 30° off-axis. (In the wide-beam case the difference between Legendre function and cosine shading is quite small, so we do not show a comparison in that case.)

3.2 Full-Sphere Radiation Patterns

For the two shading functions considered above, Fig. 8 shows 3D radiation patterns (polar balloons) calculated at several frequencies, via numerical quadrature of the integral in eq. (3), and normalized to the on-axis ($\theta = \phi = 0$) response. For ease of presentation, and to facilitate comparison with Keele's results [8, 9], the array plane (i.e. the xy-plane) is oriented vertically.

As expected, in both cases there is a transition from monopole radiation at low frequency to a frequency-independent radiation pattern above the cutoff frequency.

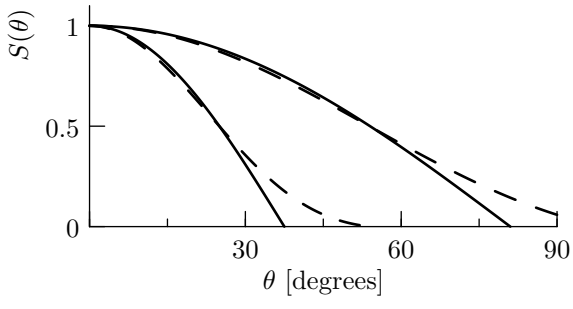

Fig. 4: Shading functions with -6 dB beam angles of 25° and 47°, via cosine shading [solid] and Chebyshev shading [dashed]. The degree-6 Chebyshev polynomial (20) was used for the narrow beam; a degree-2 polynomial was used for the wider beam.

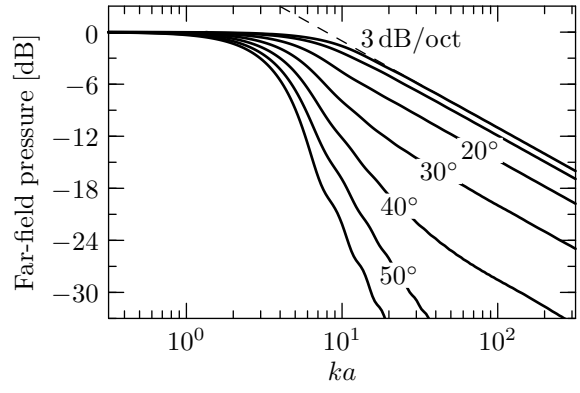

Fig. 5: Raw (unequalized) far-field magnitude response at various angles θ in the plane of an array with the Chebyshev shading (20).

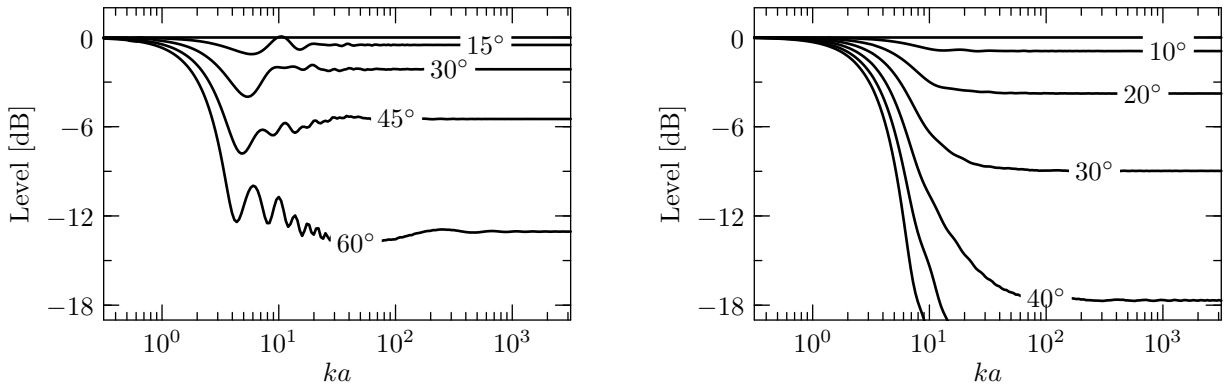

(a) Wide Beam (b) Narrow Beam

Fig. 6: Far-field magnitude responses at various angles θ in the plane of the array, normalized to the on-axis ($\theta = 0$) response, for (a) a wide-beam array with the cosine shading of eq. (19), and (b) a narrow-beam array with the Chebyshev shading of eq. (20).

Above cutoff the full radiation pattern is remarkably constant in both cases, except near the z-axis where the pattern settles down only at the highest frequencies. In agreement with eq. (14), the limiting pattern in the plane of the array is determined by the shading function, while the out-of-plane pattern has a broad $1/\sqrt{\cos\phi}$ shape with corresponding amplitude peaks on the z-axis. As predicted, the radiation patterns are bi-directional and symmetric front-to-back (i.e. across the yz-plane).

3.3 Directivity Index

The directivity index [2] characterizes the directivity of a radiation pattern $p(r,\theta,\phi)$ in terms of the ratio of the on-axis intensity to that of a point source radiating the same total power. For the coordinate system of Fig. 1 the directivity index is given by

$$\mathrm{DI} = 10\log_{10}\frac{4\pi|p(r,0,0)|^2}{\int_0^{2\pi}\int_{-\pi/2}^{\pi/2}|p(r,\theta,\phi)|^2\cos\phi\,d\phi\,d\theta}. \quad (21)$$

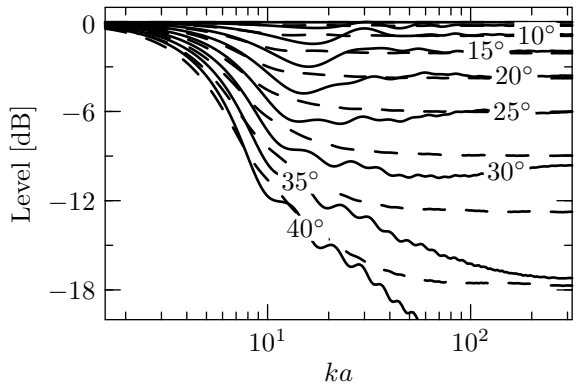

Fig. 7: Far-field magnitude responses at various angles θ in the plane of the array, normalized to the on-axis ($\theta = 0$) response, for arrays with -6 dB beam angle of 25° via Legendre function shading [solid] and the Chebyshev shading (20) [dashed]. Angular resolution is 5°.

Fig. 9 shows the directivity index as a function of dimensionless frequency ka, calculated by numerical quadrature of (21) with the radiation pattern given by eq. (3), for several different choices of array shading. As expected, all four examples give 0 dB directivity (monopole radiation) at low frequency, with increasing directivity in a transition band around the cutoff frequency of the array, above which the directivity becomes constant and determined by the array shading. For the wide-beam arrays in particular the directivity index is remarkably constant, varying by less then a few dB over the entire spectrum. Also, Fig. 9 gives further confirmation that our Chebyshev polynomial shading gives a small improvement over Legendre function shading, with more consistent directivity (less ripple) above the cutoff frequency.

The limiting constant value of the directivity above cutoff can be found by substituting eq. (15) into (21), which gives

$$\mathrm{DI} = 10\log_{10}\frac{|S(0)|^2}{\int_0^{\pi/2}|S(\theta)|^2\,d\theta} \quad (ka \gg n_{\max}). \quad (22)$$

In the case of cosine shading (eq. (17)) this simplifies to $\mathrm{DI} = 10\log_{10}(2/\theta_0)$; when the arc coverage θ_0 is decreased by half, the directivity index increases 3 dB.

4 Discrete Arrays

Our theory has so far assumed a continuous line source. An array of discrete source elements (as is likely to be used in a practical implementation) can only approximate this condition. As a simple model of the discrete case, here we consider a circular-arc array of discrete point sources with amplitude shading determined by sampling a given shading function. The behavior of such an array can be predicted by applying the modal theory developed in Sec. 1. Further results on aliasing and grating-lobe effects in circular arrays can be found in [13, 15, 31].

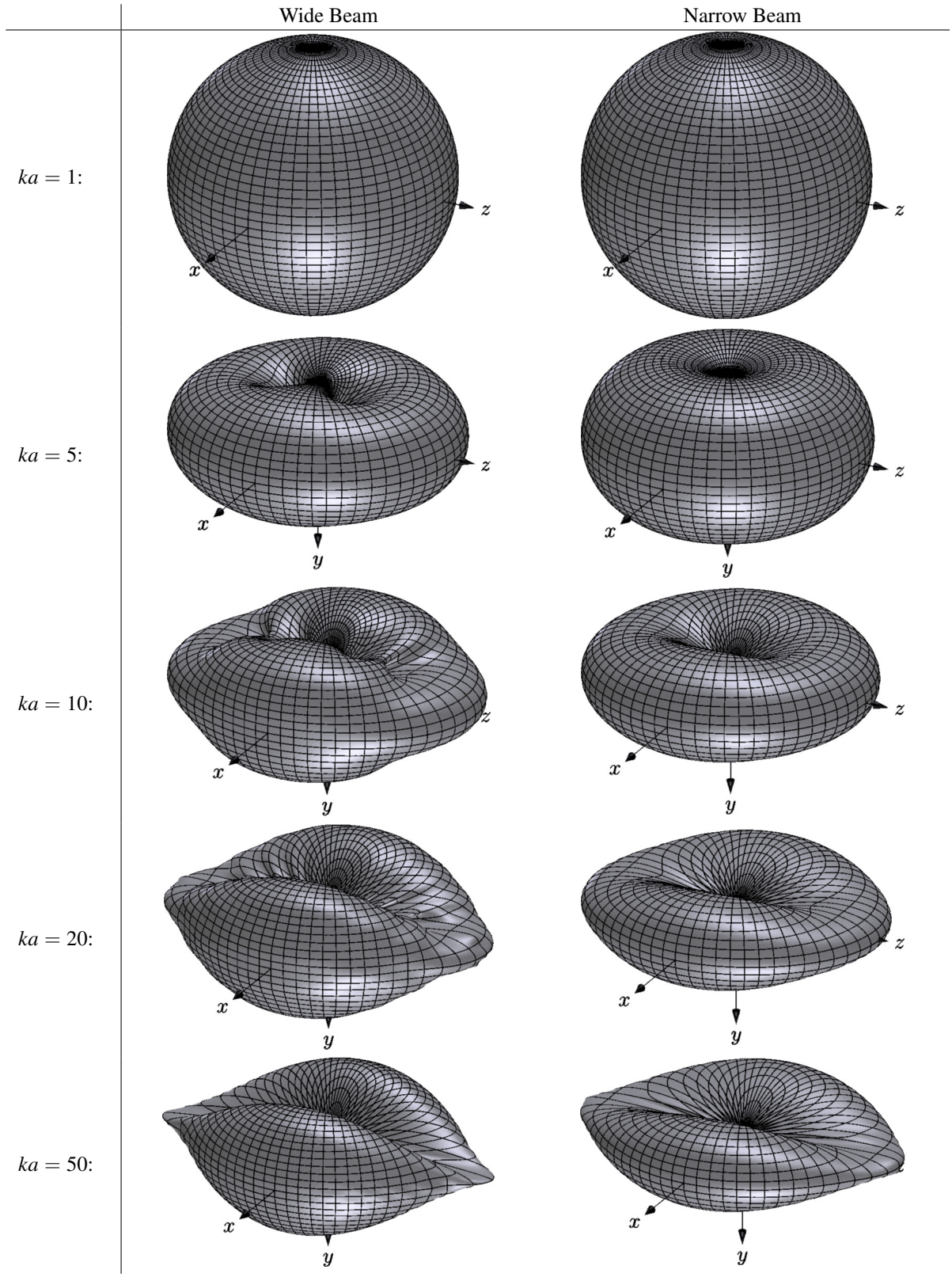

Fig. 8: 3D radiation patterns (polar balloons) for circular-arc arrays with the wide-beam cosine shading of eq. (19) and narrow-beam Chebyshev shading of eq. (20). All plots are normalized on-axis. Note that the array orientation differs from Fig. 1: in the interests of space and comparison with [9], the array plane (the *xy*-plane) is oriented vertically here.

Consider an amplitude-shaded circular array of N point sources spaced uniformly around the circle at angles

$$\alpha_j = j\frac{2\pi}{N} \quad (j = 0,\ldots,N-1), \tag{23}$$

with strengths $S(\alpha_j)$ determined by sampling the shading function $S(\alpha)$. (In a circular-arc array most of the sources will have zero strength and so can be eliminated in practice). We can represent such an array by the shading function

$$\hat{S}(\alpha) = \frac{2\pi}{N}\sum_{j=0}^{N-1} S(\alpha_j)\delta(\alpha-\alpha_j) \tag{24}$$

where δ is the Dirac delta distribution. One can show (e.g. directly via eq. (4) or by convolution properties of the discrete Fourier transform [35]) that $\hat{S}$ has cosine series coefficients

$$\hat{a}_n = a_n + \sum_{k=\pm1,\pm2,\ldots} (a_{n+kN} + a_{-n+kN}). \tag{25}$$

Thus the mode amplitudes in the discrete and continuous cases are identical, except that discretization excites additional higher-order spurious modes (represented by the sum on the right). Eq. (25) appears in various forms throughout the literature on circular arrays [13, 27, 28, 31, 36] and discrete sampling of periodic signals more generally.

Fig. 10 illustrates the Fourier spectrum of a typical continuous shading $S(\alpha)$ together with that of its discretization $\hat{S}(\alpha)$. As before, $n_{\max}$ is the index of the highest-order non-negligible mode of the continuous shading. Provided that $N \geq 2n_{\max}$, it follows from eq. (25) that there will be no spectral overlap between the spurious modes and those of the continuous shading (i.e. spatial aliasing), so that the shading mode amplitudes a_n and $\hat{a}_n$ will be *identical* for all $n \leq N/2$ (this is a special case of the well-known Nyquist-Shannon sampling theorem, applied to sampling in space rather than time).

Assuming this Nyquist condition is met, the continuous and discrete arrays will behave indistinguishably for frequencies $ka \ll N - n_{\max}$. At these frequencies the spurious modes are all strongly attenuated in the far field (recall that a radiation mode of order n rolls off at $6n$ dB/oct at low frequency) so that only the low-order shading modes contribute to the radiation pattern. Since the low-order mode amplitudes are identical in the continuous and discrete cases, their radiating behaviors are identical. Only at higher frequencies $ka \gtrsim N - n_{\max}$ do the spurious modes begin to radiate, appearing as grating lobes in the radiation pattern. Note that $ka \approx N$ when the element spacing and acoustic wavelength are approximately equal; thus grating lobes are avoided if the element spacing is small compared with the wavelength, as might be anticipated on physical grounds.

As an illustrative example, Fig. 11 plots far-field magnitude responses at various angles in the plane of an array of $N = 50$ point sources with the Chebyshev shading of eq. (20). (Only 15 of the sources are actually active; the remainder lie in the part of the circle where the shading function is zero.) The responses were calculated using the formula

$$|p(r,\theta)| = \frac{1}{r}\left|\sum_{j=0}^{N-1} S(\alpha_j)e^{ika\cos(\theta-\alpha_j)}\right| \tag{26}$$

which results from substituting the discrete shading of eq. (24) into eq. (3). Comparison with Fig. 5 shows that, as expected, for all frequencies up to $ka \approx N = 50$ the response of the discrete array is indistinguishable from that of a continuous array with the same shading. At higher frequency the spurious modes due to discretization begin to radiate, resulting in loss of pattern control. In this example the constant directivity bandwidth (from cutoff to the appearance of grating lobes) is about one decade. From the theory developed above we can see that, in general, the constant directivity bandwidth will be about $N/n_{\max}$.

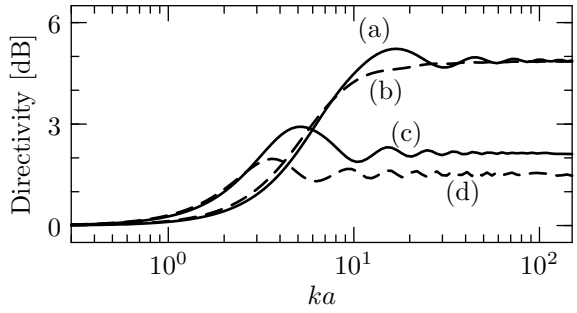

Fig. 9: Directivity index as a function of frequency, for circular-arc arrays with several different shading functions: (a) Legendre function shading from [8] with -6 dB beam angle of 25°; (b) the degree-6 Chebyshev polynomial shading of eq. (20); (c) the wide-beam cosine shading of eq. (19); (d) degree-2 Chebyshev polynomial shading to achieve the same -6 dB beam width as (c).

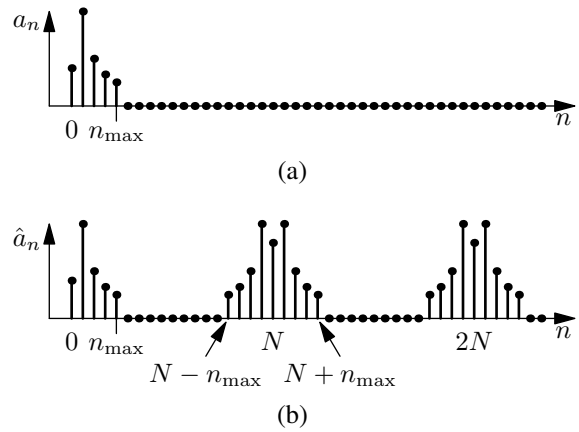

Fig. 10: Mode amplitudes (Fourier cosine series coefficients) a_n of (a) a given continuous shading function $S(\alpha)$, and (b) the sampled discrete shading $\hat{S}(\alpha)$ in eq. (24).

5 Conclusion

We have developed a far-field theory that accounts for the observed [8, 9, 10, 11] constant directivity behavior of amplitude-shaded circular-arc line arrays. The key to understanding and optimizing such arrays is to express the shading function as a Fourier cosine series (expansion in circular harmonics). This yields a modal theory that can be used to predict the radiating behavior at all frequencies. The conclusions that follow are remarkably parallel to those for an amplitude-shaded spherical cap, as developed in [4, 5]:

- Provided the active part of the array is limited to an arc of 180° or less, the radiation pattern is asymptotically frequency-independent above a cutoff frequency determined by the arc radius and the highest-order non-negligible shading mode. The cutoff frequency is inversely proportional to the arc radius and prescribed beam width.
- Above cutoff the constant radiation pattern is bi-directional, and can be represented as a product of in-plane and out-of-plane patterns. The in-plane pattern is identical to the given shading function, while the out-of-plane pattern has a broad $1/\sqrt{\cos\phi}$ form with a strong amplitude peak within a small solid angle around the axis of the circular arc ($\phi \approx \pm\frac{\pi}{2}$).
- Above cutoff the magnitude response rolls off at 3 dB/oct, everywhere in the far field.
- Directivity control is lost below cutoff: the radiation pattern becomes omni-directional when the array becomes acoustically small.

These theoretical results are corroborated by Keele's earlier measurements and simulations [9, 10, 12] as well as the simulations presented here.

Our theory indicates how to design the amplitude shading so as to achieve constant directivity over the widest band possible: the Fourier spectrum of the shading function must be concentrated in its lowest-order terms. This explains Keele's observations that shading with a Legendre function (borrowed from [4]) behaves very well, but it also opens the way to designing better shading functions. Here we have developed two new shading functions adapted to circular-arc arrays: one based on a simple cosine form, the other based on Chebyshev polynomials. Cosine shading has the advantage of being quite simple, and allows for the widest beam pattern. Chebyshev polynomial shading gives a better-controlled frequency response, at the expense of requiring greater arc coverage for a given beam width.

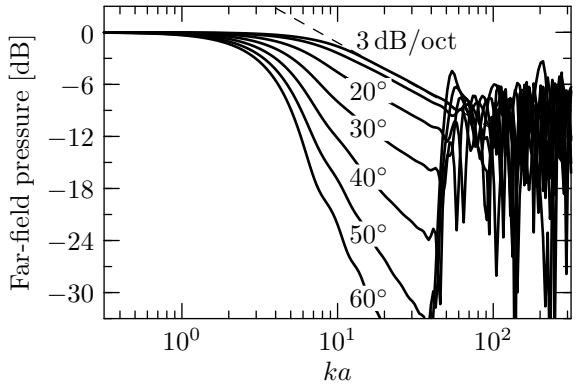

Fig. 11: Raw (unequalized) far-field magnitude responses in the plane of an array of $N = 50$ discrete point sources with uniform angular spacing and the Chebyshev shading of eq. (20).

Our main results are based on a theory for a continuous circular-arc line source. However, such a source can be well-approximated by a discrete array of point sources with uniform angular spacing and amplitude shading determined by sampling the shading function. This discretization introduces high-order spatial modes, but our theory predicts that these are strongly attenuated in the far field except at high frequencies. When the frequency increases to where the element spacing is on the order of the acoustic wavelength, the high-order modes begin to radiate and appear as grating lobes in the radiation pattern, resulting in loss of directivity control.

As for other array geometries, directivity control by a circular-arc array is limited to the frequency band in which the wavelength is both smaller than the array size (arc length) and larger than the element spacing. Unlike other array geometries, however, a circular-arc array radiates a pattern that is remarkably constant throughout this band: a linear array, for example, has a beam pattern that inherently narrows with increasing frequency. Moreover, unlike the baffled circular arrays considered in [23, 24, 25, 26, 27, 28] an unbaffled circular arc facilitates construction of long arrays, especially in a ground-plane deployment [11, 12] which doubles the effective array length, extending the constant-directivity bandwidth by one octave: a 2 m tall ground-plane arc array is effectively 4 m long and thereby exhibits directivity control starting below 100 Hz.

Practical implementation of our theory is beyond the scope of the present paper. Several engineering issues arise, including departure of source elements from ideal point-source behavior, mutual coupling between source elements, source mismatch in both amplitude and phase, electronic implementation of the shading function, and equalization of the inherent −3 dB response. Some of these issues and more have been addressed in the literature previously [10, 11, 12, 31], including some results indicating that our theory can be extended to include directional elements [14, 15]. However, a number of open questions remain to be investigated.

A major benefit of CBT spherical-cap arrays, shown theoretically in [4], is that *both* the near- and far-field radiation pattern agree with the shading function, and thus there is no essential difference between the near- and far-field behaviors. Unfortunately the (far-field) theory presented here does not account for this important aspect of circular-arc line arrays; we plan to address this issue in future work.

6 Acknowledgements

The authors are grateful to the anonymous reviewers who worked through many of the tedious mathematical details and offered constructive criticisms that resulted in a much-improved manuscript. Richard Taylor and Kurtis Manke were supported by Thompson Rivers University via a scholarship from the Undergraduate Research Experience Award Program.

7 REFERENCES

[1] R. Taylor, D. B. Keele, Jr., "Theory of constant directivity circular-arc line arrays," presented at the *Aud. Eng. Soc. Convention 143* (2017 Oct.).

[2] L. L. Beranek, T. J. Mellow, *Acoustics: Sound Fields and Transducers* (Academic Press) (2012), https://doi.org/10.1016%2Fb978-0-12-391421-7.00004-x.

[3] F. Toole, *Sound Reproduction: The Acoustics and Psychoacoustics of Loudspeakers and Rooms* (Focal Press) (2008), https://doi.org/10.4324%2F9780080888019.

[4] P. H. Rogers, A. L. Van Buren, "New approach to a constant beamwidth transducer," *J. Acoust. Soc. Am.*, vol. 64, no. 1, pp. 38–43 (1978), https://doi.org/10.1121%2F1.381954.

[5] J. Jarzynski, W. J. Trott, "Array shading for a broadband constant directivity transducer," *J. Acoust. Soc. Am.*, vol. 64, no. 5, pp. 1266–1269 (1978), https://doi.org/10.1121%2F1.382110.

[6] D. B. Ward, R. A. Kennedy, R. C. Williamson, "Constant Directivity Beamforming," in M. Brandstein, D. Ward (Eds.), *Microphone Arrays: Signal Processing Techniques and Applications*, chap. 1 (Springer) (2013), https://doi.org/10.1007%2F978-3-662-04619-7_1.

[7] H. Teutsch, *Modal Array Signal Processing: Principles and Applications of Wavefield Decomposition* (Springer) (2007).

[8] D. B. Keele, Jr., "The application of broadband constant beamwidth transducer (CBT) theory to loudspeaker arrays," presented at the *Aud. Eng. Soc. Convention 109* (2000 Sep.).

[9] D. B. Keele, Jr., "The full-sphere sound field of constant beamwidth transducer (CBT) loudspeaker line arrays," *J. Aud. Eng. Soc.*, vol. 51, no. 7/8, pp. 611–624 (2003 Jul.).

[10] D. B. Keele, Jr., "Practical implementation of constant beamwidth transducer (CBT) loudspeaker circular-arc line arrays," presented at the *Aud. Eng. Soc. Convention 115* (2003 Oct.).

[11] D. B. Keele, Jr., D. J. Button, "Ground-plane constant beamwidth transducer (CBT) loudspeaker circular-arc line arrays," presented at the *Aud. Eng. Soc. Convention 119* (2005 Oct.).

[12] D. B. Keele, Jr., "Use of ground-plane constant beamwidth transducer (CBT) loudspeaker line arrays for sound reinforcement," presented at the *Aud. Eng. Soc. Convention 141* (2016 Oct.).

[13] R. C. Hansen, *Phased Array Antennas* (Wiley), 2nd ed. (2009), https://doi.org/10.1002%2F9780470529188.

[14] R. J. Mailloux, *Phased Array Antenna Handbook* (Artech House, Boston), 2nd ed. (2005).

[15] L. Josefsson, P. Persson, *Conformal Array Antenna Theory and Design* (Wiley) (2006), https://doi.org/10.1002%2F047178012x.

[16] S. W. Lee, Y. T. Lo, "On the pattern function of circular arc arrays," *IEEE Trans. Antennas Propag.*, vol. 13, no. 4, pp. 649–650 (1965), http://dx.doi.org/10.1109/TAP.1965.1138469.

[17] J. K. Butler, "Radiation from circular arc antenna arrays," *Radio Science*, vol. 4, no. 6, pp. 539–544 (1969), http://dx.doi.org/10.1029/RS004i006p00539.

[18] M. S. Ureda, "Analysis of loudspeaker line arrays," *J. Aud. Eng. Soc.*, vol. 52, no. 5, pp. 467–495 (2004 May).

[19] Yong Wang, Yixin Wang, Yuanling Ma, Zhengyao He, YuKang Liu, "Broadband pattern synthesis for circular sensor arrays," *J. Acoust. Soc. Am.*, vol. 136, no. 2, pp. EL153–158 (2014), https://doi.org/10.1121%2F1.4890213.

[20] Mu PengCheng, Yin QinYe, Zhang JianGuo, "A wideband beamforming method based on directional uniform circular arrays," *Science China Information Sciences*, vol. 53, no. 12, pp. 2600–2609 (2010), https://doi.org/10.1007%2Fs11432-010-4109-3.

[21] A. Parthy, N. Epain, A. van Schaik, C. T. Jin, "Comparison of the measured and theoretical performance of a broadband circular microphone array," *J. Acoust. Soc. Am.*, vol. 130, no. 6, pp. 3827–3837 (2011), https://doi.org/10.1121%2F1.3658443.

[22] J. Meyer, "Beamforming for a circular microphone array mounted on spherically shaped objects," *J. Acoust. Soc. Am.*, vol. 109, pp. 185–193 (2001), https://doi.org/10.1121%2F1.1329616.

[23] M. Kolunžija, C. Faller, M. Vetterli, "Baffled circular loudspeaker array with broadband high directivity," presented at the *IEEE International Conference on Acoustics Speech and Signal Processing (ICASSP)*, pp. 73–76 (2010 Apr.), https://doi.org/10.1109%2Ficassp.2010.5496204.

[24] M. Møller, M. Olsen, F. Agerkvist, J. Dyreby, G. Munch, "Circular loudspeaker array with controllable directivity," presented at the *Aud. Eng. Soc. Convention 128* (2010 May).

[25] M. Kolundžija, C. Faller, M. Vetterli, "Design of a compact cylindrical loudspeaker array for spatial sound reproduction," presented at the *Aud. Eng. Soc. Convention 130* (2011 May).

[26] F. M. Fazi, M. Shin, F. Olivieri, S. Fontana, L. Yue, "Comparison of pressure-matching and mode-matching beamforming methods for circular loudspeaker arrays," presented at the *Aud. Eng. Soc. Convention 137* (2014 Oct.).

[27] F. M. Fazi, M. Shin, F. Olivieri, S. Fontana, "Low frequency performance of circular loudspeaker arrays," presented at the *Aud. Eng. Soc. Convention 138* (2015 May).

[28] H. Teutsch, W. Kellerman, "Acoustic source detection and localization based on wavefield decom-

position using circular microphone arrays," *J. Acoust. Soc. Am.*, vol. 120, no. 5, pp. 2724–2736 (2006), https://doi.org/10.1121/1.2346089.

[29] F.-M. Hoffmann, E. G. Williams, F. M. Fazi, S. Fontana, "An analytical model for wedge-shaped acoustic arrays," *J. Sound Vib.*, vol. 439, pp. 56–76 (2019), https://doi.org/10.1016/j.jsv.2018.09.041.

[30] P. M. Morse, K. U. Ingard, *Theoretical Acoustics* (Princeton University Press) (1987).

[31] D. E. N. Davies, "Circular Arrays," in A. W. Rudge, K. Milne, A. D. Olver, P. Knight (Eds.), *The handbook of antenna design*, vol. 2, chap. 12 (Peter Peregrinus) (1983), https://doi.org/10.1049%2Fpbew015g_ch12.

[32] "*NIST Digital Library of Mathematical Functions*," http://dlmf.nist.gov, Release 1.0.18 of 2018-03-27 [accessed 23-May-2018], F. W. J. Olver, A. B. Olde Daalhuis, D. W. Lozier, B. I. Schneider, R. F. Boisvert, C. W. Clark, B. R. Miller and B. V. Saunders, eds.

[33] I. D. Longstaff, P. E. K. Chow, D. E. N. Davies, "Directional properties of circular arrays," *Proc. IEE*, vol. 114, no. 6, pp. 713–718 (1967 Jun.), https://doi.org/10.1049/piee.1967.0142.

[34] L. Powell, "Systematic design of accurate pink noise filters," presented at the *Aud. Eng. Soc. Convention 69* (1981 May).

[35] A. V. Oppenheim, R. W. Schafer, *Discrete-Time Signal Processing* (Pearson), 3rd ed. (2010).

[36] M. Poletti, T. Betlehem, "Design of a prototype variable directivity loudspeaker for improved surround sound reproduction in rooms," presented at the *AES 52nd International Conference: Sound Field Control – Engineering and Perception* (2013 Sep.).

[37] N. L. Carothers, *A short course on approximation theory* (Bowling Green State University, Bowling Green, OH) (1998), https://bit.ly/2MmIQbZ [accessed 11-Sep-2018].

[38] T. J. Rivlin, *An Introduction to the Approximation of Functions* (Dover) (1969).

A.1 Half-Circle Restriction

Theorem 1. *Let $(a_n)_{n=0}^{\infty}$ be the sequence of Fourier cosine series coefficients of the function $S(\theta) = \sum_{n=0}^{\infty} a_n \cos n\theta$ and let*

$$S_e(\theta) = \sum_{n \text{ even}} a_n \cos n\theta, \quad S_o(\theta) = \sum_{n \text{ odd}} a_n \cos n\theta.$$

Let θ be given. Then $|S_o(\theta)| = |S_e(\theta)|$ if and only if at most one of $S(\theta)$ and $S(\pi-\theta)$ is non-zero.

Proof

For any θ we have

$$\begin{aligned} S_o(\pi-\theta) &= \sum_{n \text{ odd}} a_n \cos n(\pi-\theta) \\ &= \sum_{n \text{ odd}} a_n (-1)^n \cos n\theta = -S_o(\theta) \end{aligned} \tag{A.1}$$

and similarly

$$S_e(\pi-\theta) = \sum_{n \text{ even}} a_n (-1)^n \cos n\theta = S_e(\theta). \tag{A.2}$$

Thus we have

$$\begin{cases} S(\theta) & = S_e(\theta) + S_o(\theta) \\ S(\pi-\theta) & = S_e(\theta) - S_o(\theta) \end{cases}$$

which implies

$$\begin{cases} 2S_e(\theta) = S(\theta) + S(\pi-\theta) \\ 2S_o(\theta) = S(\theta) - S(\pi-\theta). \end{cases} \tag{A.3}$$

It follows that

$$\begin{aligned} &|S_e(\theta)| = |S_o(\theta)| \\ &\iff |S(\theta) + S(\pi-\theta)| = |S(\theta) - S(\pi-\theta)| \\ &\iff S(\theta) + S(\pi-\theta) = \pm\big(S(\theta) - S(\pi-\theta)\big) \\ &\iff S(\theta) = 0 \text{ or } S(\pi-\theta) = 0. \end{aligned}$$

This completes the proof.

Eqs. (A.1)–(A.2) show that in general the functions $S_o(\theta)$, $S_e(\theta)$ have odd and even symmetry, respectively, about $\theta = \pm\frac{\pi}{2}$. In the body of the paper (cf. eq. (14)) this implies that the limiting radiation pattern above cutoff is bi-directional and symmetric across the yz-plane. If $S(\theta)$ is non-zero only for $-\frac{\pi}{2} < \theta < \frac{\pi}{2}$ then eq. (A.3) gives

$$|S_e(\theta)| = \begin{cases} \frac{1}{2}|S(\theta)| & \text{if } -\frac{\pi}{2} < \theta < \frac{\pi}{2} \\ \frac{1}{2}|S(\pi-\theta)| & \text{if } \frac{\pi}{2} < \theta < \frac{3\pi}{2}. \end{cases} \tag{A.4}$$

A.2 Cosine Shading

To derive an optimal shading for circular-arc arrays, here we adapt the technique that was used in [4] to derive Legendre function shading for a spherical cap. We seek an even shading function

$$S(\theta) = \begin{cases} f(\theta) & |\theta| \le \theta_0 \\ 0 & \theta_0 < |\theta| \le \pi \end{cases} \tag{A.5}$$

where the arc half-angle $\theta_0 \le \frac{\pi}{2}$ is given and f is a function to be determined. The cosine series coefficients of S are then

$$a_n = \frac{2}{\pi} \int_0^{\theta_0} f(\theta) \cos(n\theta)\, d\theta \qquad (n > 0). \tag{A.6}$$

To concentrate this Fourier spectrum in its lowest-order terms, our strategy is to determine f so that a_n^2 is minimized (as a function of θ_0) for all $n > N$, while the a_n^2 are maximized for $n \le N$.

Making all the a_n stationary with respect to θ_0 requires that

$$0 = \frac{da_n}{d\theta_0} = \frac{2}{\pi} f(\theta_0) \cos(n\theta_0). \tag{A.7}$$

Satisfying this equation for all n requires $f(\theta_0) = 0$, i.e. f should have a root at the arc endpoint θ_0. We take this to be the *smallest* such root, since the beam pattern would otherwise have undesirable side-lobes. We can then assume without loss of generality that $f(\theta) > 0$ for $0 < \theta < \theta_0$.

To distinguish whether the a_n^2 are maximized or minimized as a function of θ_0 we employ the second derivative test; to this end we evaluate

$$\frac{d^2 a_n^2}{d\theta_0^2} = \frac{4}{\pi} a_n f'(\theta_0)\cos(n\theta_0). \tag{A.8}$$

Let N be the integer such that for all $n \le N$ the smallest root of $\cos(n\theta)$ is greater than θ_0, while for $n > N$ the smallest root is less than θ_0. Thus,

$$N = \lfloor \pi/(2\theta_0) \rfloor \tag{A.9}$$

where $\lfloor \cdot \rfloor$ denotes the integer part. Then for $n \le N$ we have $\cos(n\theta) > 0$ on $[0, \theta_0]$, hence $a_n > 0$ by eq. (A.6). Assuming $f'(\theta_0) < 0$ gives $d^2 a_n^2/d\theta_0^2 < 0$, so that each of the a_n^2 $(n \le N)$ is indeed a local *maximum* as a function of θ_0.

Now we need to ensure that a_n^2 is a local *minimum* as a function of θ_0 for all $n > N$, which would require $d^2 a_n^2/d\theta_0^2 > 0$. Thus, from eq. (A.8) we require

$$\cos(n\theta_0) \int_0^{\theta_0} f(\theta)\cos(n\theta)\, d\theta < 0 \quad (n > N). \tag{A.10}$$

This gives the shading function

$$f(\theta) = \cos\left(\tfrac{\pi}{2} \cdot \tfrac{\theta}{\theta_0}\right). \tag{A.11}$$

as one possible choice that satisfies (A.10) together with our various other assumptions. Indeed, we have

$$\begin{aligned} &\cos(n\theta_0) \int_0^{\theta_0} f(\theta)\cos(n\theta)\, d\theta \\ &\qquad = \frac{\left(\frac{\pi}{2\theta_0}\right)^2}{\left(\frac{\pi}{2\theta_0}\right)^2 - n^2} \cdot \cos^2(n\theta_0) < 0 \end{aligned} \tag{A.12}$$

when $n > N = \lfloor \pi/(2\theta_0) \rfloor$ so that (A.10) is satisfied and a_n^2 is indeed a local minimum, as a function of θ_0, for all $n > N$. Thus the cosine function (A.11) is (in one particular sense) an optimal choice of shading function.

A.3 Chebyshev Polynomial Shading

Here we take a different (in some ways better) approach to optimally shading a circular-arc array to achieve broadband constant directivity. Again we seek a shading function $S(\theta)$ of the form (A.5) but employ the following strategy to obtain such a function whose cosine series is concentrated in its lowest-order terms. Let $f(\theta)$ be a low-order polynomial in $\cos\theta$, chosen so that $f(\theta)$ vanishes as nearly as possible for $\theta_0 \le |\theta| \le \pi$. When set $f(\theta)$ to 0 on this interval to form $S(\theta)$ as in (A.5), this introduces higher-order spectral terms but these have small magnitude (since the change in f is small). Thus the Fourier spectrum of S remains concentrated in its lowest orders.

To this end, let $S(\theta)$ be given by (A.5) where

$$f(\theta) = P(\cos\theta) \tag{A.13}$$

and P is a degree-N polynomial to be determined. With $z = \cos\theta$ we want the maximum of $|P(z)|$ on the interval $[-1, \cos\theta_0]$ to be as small as possible (so that $P(\cos\theta)$ is minimized for $\theta_0 \le |\theta| \le \pi$). It is a well-known result in approximation theory that this criterion uniquely determines P and that (as elaborated in the following) P can be expressed in terms of a Chebyshev polynomial [37, ch. 4]. Alas, the reasons for this are not readily summarized; the interested reader is referred to e.g. [37, 38] or any standard reference on approximation theory or numerical analysis.

The first few Chebyshev polynomials $T_N(u)$ are given, up to a multiplicative constant, by

$$\begin{aligned} &T_1(u) = u, \qquad T_3(u) = 4u^3 - 3u, \\ &T_2(u) = 2u^2 - 1, \; T_4(u) = 8u^4 - 8u^2 + 1. \end{aligned} \tag{A.14}$$

Each T_N is the (unique) monic polynomial of degree N whose maximum absolute value on $[-1, 1]$ is a minimum [37, p. 36]. Moreover [38], among all degree-N polynomials T_N has largest values outside the interval $[-1, 1]$.

To obtain the polynomial $P(\cos\theta)$ that vanishes as nearly as possible for all $\theta_0 \le |\theta| \le \pi$, following [37, Cor. 4.1.1] we let $z = \cos\theta$ and form $P(\cos\theta) = T_N(u(z))$ where

$$u(z) = 2 \cdot \frac{1+z}{1+\cos\theta_0} - 1$$

is the linear map that takes $z \in [-1, \cos\theta_0]$ to $u \in [-1, 1]$. This gives the shading function (A.5) in which

$$f(\theta) = T_N\left(2 \cdot \frac{1+\cos\theta}{1+\cos\theta_0} - 1\right). \tag{A.15}$$

Being "close" to a degree-N polynomial in $\cos\theta$, this shading function has its cosine series concentrated in its lowest-order terms.

THE AUTHORS

Richard Taylor

Kurtis Manke

D. B. (Don) Keele, Jr.

Richard Taylor is a Senior Lecturer in mathematics and physics at Thompson Rivers University, Canada, where he has been employed since 2005. He holds a Ph.D. in Applied Mathematics (2004) from the University of Waterloo, Canada, as well as a B.Sc. in Physics (1998) and M.Sc. in Geophysics (1999) from the University of British Columbia, Canada. His main research interests are physical acoustics, loudspeaker arrays, digital signal processing, dynamical systems, and scientific computing.

●

Kurtis Manke is a Master's student in applied mathematics at the University of Victoria, Canada. He holds a B.Sc. in Physics (2017) from Thompson Rivers University, Canada. His main research interests are mathematical epidemic models and loudspeaker arrays.

●

D. B. (Don) Keele, Jr. was born in Los Angeles, California, on 1940 Nov. 2. After serving in the U.S. Air Force for four years as an aircraft electronics navigation technician, he attended California State Polytechnic University at Pomona, where he graduated with honors and B.S. degrees in both electrical engineering and physics. He received an M.S. degree in electrical engineering with a minor in acoustics from the Brigham Young University, Provo, Utah, in 1975.

Mr. Keele has worked for a number of audio-related companies in the area of loudspeaker R&D and measurement technology, including Electro-Voice, Klipsch, JBL, and Crown International. He holds eight patents. For 11 years he wrote for Audio magazine as a senior editor performing loudspeaker reviews.

Mr. Keele has presented and published over 56 technical papers on loudspeaker design and measurement methods and related topics. He is a frequent speaker at AES section meetings and workshops and has chaired several AES technical paper sessions. He is an AES fellow (for contributions to the design and testing of low-frequency loudspeakers), a past member of the JAES Review Board, past member of the AES Board of Governors, and past AES vice president, Central Region USA/Canada. Mr. Keele has received several honors and awards: the 1975 AES Publications Award, the 2001 TEF Richard C. Heyser Award, the Scientific and Technical Academy Award in 2002 from the Academy of Motion Picture Arts and Sciences (for his work on cinema constant-directivity loudspeaker systems), the 2011 The Beryllium Driver Award for Lifetime Achievement, and the 2016 AES Gold Medal Award. He is listed in the AES Audio Timeline for his pioneer work on the design of constant-directivity high-frequency horns in 1974.